Optica Applicata, Vol. XLVII, No. 2, 2017
DOI: 10.5277/oa170211

Ultrashort pulse propagation recording by using the transmission-type light in flight holography

YUPENG FAN[1, 2], JINGZHEN LI[1*], SHUIQIN ZHENG[1], XIAOWEI LU[1], XIAOPIN ZHONG[3]

[1]Shenzhen Key Laboratory of Micro-Nano Photonic Information Technology, College of Electronic Science and Technology, Shenzhen University, Shenzhen 518060, P.R. China

[2]College of Optoelectronics Engineering, Shenzhen University, Shenzhen 518060, P.R. China

[3]Shenzhen Key Laboratory of Electromagnetic Control, Shenzhen University, Shenzhen 518060, P.R. China

[*]Corresponding author: lijz@szu.edu.cn

In this paper, the distortion of the reconstructed images of the propagating light pulse in transmission light-in-flight holography recording was analyzed. Based on the analysis model, for recording the wavefront more accurately, the optimized selection of relevant parameters was made. Furthermore, a cylindrical lens was introduced to correct the image distortion. Additionally, the light-in-flight recording of the wavefront changing during propagation was simulated.

Keywords: light in flight, visualization of pulse propagation, holography.

1. Introduction

In 1978, ABRAMSON proposed the fundamental theory of light-in-flight (LIF) and performed the first practical experiment by using a laser with short coherence length [1]. Since then, the LIF was used in applications such as optical fiber testing [2], measurement of the shape and deformation of a 3D object [3], the study of wind tunnel flows [4], chrono-coherent imaging (CCI) for medicine [5], and so on. Besides, AWATSUJI and co-workers recorded and observed, for the first time, 3D image of propagating femtosecond light pulse as continuous moving picture using LIF recording by holography [6].

The LIF recording by holography is a technique to obtain a time-resolved image of the propagating light and is used as a time-gated viewing system for ultrafast phenomena. To record a hologram, the laser pulse is divided into two beams. One is used to illuminate the object and the other acts as the reference beam. In order to extract valuable infor-

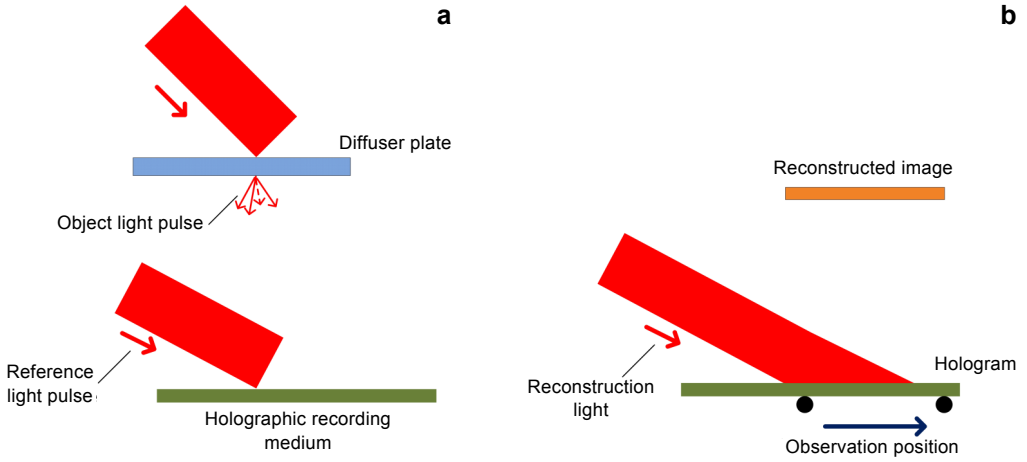

Fig. 1. Schematic of recording (**a**) and reconstruction (**b**) arrangements.

mation about the test object, the diffuser plate is attached to the test object. When a light pulse propagates inside the test object, the scattered light pulse from the diffuser surface is used as the object pulse. Only the parts where the optical path difference (OPD) between the laser beam to the holographic plate via the object and the reference beam is shorter than the coherence length of the laser pulse used for the recording can be recorded. If the reference beam is incident obliquely to the holographic plate, its arrival time varies from point-to-point on the hologram, and different parts of hologram record the pulse front at different time, so it is possible to obtain a time resolved picture of the object wave along the transverse axis of the hologram, as shown in Fig. 1**a**.

As shown in Fig. 1**b**, the propagating pulse front can be reconstructed by illuminating the hologram with the reference pulse or continuous laser, and each different portion of the hologram reconstructs the image of the object wave at the corresponding time. In the LIF, the reference beam acts as an ultrafast optical gate, that is, holographic coherence shutter. Therefore, it is possible to observe a frameless, continuous motion picture of the light propagation by moving the point of observation which is horizontally along the hologram.

However, the distortion of a shape of the reconstructed images is an obstacle to the accuracy of LIF recording. In this paper, based on the analysis of the distortion, the selection of relevant parameters was made for recording more accurately, and a cylindrical lens was introduced to correct the distortion. Additionally, the simulation of wavefront changing during propagation was made.

2. Simulation of invariable wavefront recording

In transmission LIF, a sheet of ground glass is used to scatter the light pulse, and the scattering surface of ground glass is set as the object plane. The diffuser plate and the recording material are placed parallel to each other. After being expanded and colli-

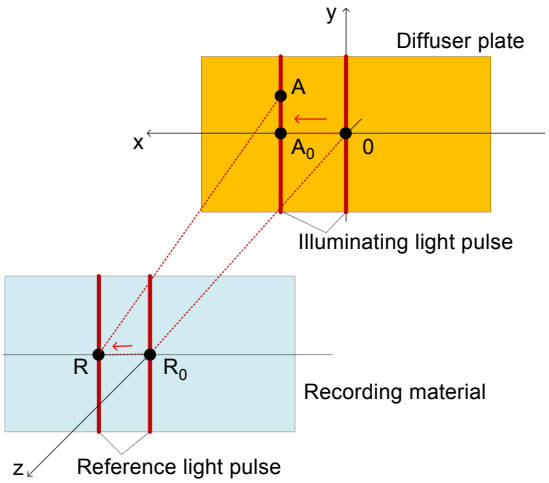

Fig. 2. Simulation model in [7].

mated, the parallel pulse is incident to the scattering surface of ground glass and recording material. A bright line is projected on the ground glass, which shows the cross -section of the pulse on the object plane.

For simplicity, we assumed that the cross-section is a straight line and is invariable during the propagation in a homogeneous medium, as shown in Fig. 2 in [7]. We define the object plane as the *xy*-plane and the axis perpendicular to the diffuser plate as the *z*-axis. The illuminating light pulse and the reference light pulse are incident to the diffuser plate and the recording material at the angle of θ_O and θ_R, respectively. The refractive index of the object is n. The illuminating pulse and reference pulse propagate along the x-axis, $c/(n\sin(\theta_O))$ represents the propagation speed of the cross-section between the illuminating light pulse and diffuser plate and $c/\sin(\theta_R)$ represents the one between the reference light pulse and the recording material. For calculation simplicity we assumed that pulses scattered on different points on the object plane in different exit directions have the same optical path length through ground glass.

Assume that the object light pulse scattered at 0 propagates in the z-direction and the reference light pulse arrived at R_0 simultaneously, and the object light pulse scattered at A and the reference light pulse simultaneously arrive at R. According to the principle that the optical path length of the object light pulse and the reference light pulse is equal, we can obtain that

$$d + L_{R_0-R}\sin(\theta_R) = nL_{0-A_0}\sin(\theta_O) + L_{A-R} \tag{1}$$

where d is the distance between the diffuser plate and the recording material, L_{R_0-R}, L_{0-A_0} and L_{A-R} are the distances between R_0 and R, 0 and A_0, and A and R, respectively.

Then, considering that the OPD between the object pulse and the reference pulse is shorter than the coherence length of the laser pulse, the Eq. (1) should be

$$d + L_{R_0-R}\sin(\theta_R) = nL_{0-A_0}\sin(\theta_O) + L_{A-R} \pm L_c \tag{2}$$

where $L_c = c\Delta t$ is the coherence length of the laser pulse, Δt is the pulse width, and c is the velocity of light.

If the coordinates of A_0, R_0 and R are given, we can calculate all coordinates of A satisfying Eq. (2) at a given R, then obtain the image reconstructed from R. By changing the coordinate of R, the image reconstructed from each point whose y-coordinate is 0 on the recording material can be calculated.

3. The reconstructed wavefront distortion and selection of relevant parameters

Firstly, we assumed the simulation conditions as follows: Δt = 96 fs, d = 30 cm, $c = 3 \times 10^8$ m/s, n = 1, which are same as that in [7]. It is worth noting that θ_O and θ_R should be 3 deg rather than 0.5 deg based on the conditions such as the time interval between adjacent pictures and the size of piece of hologram for reconstruction given in [7]. Then we obtained the reconstructed images of femtosecond light pulse propagation from pieces extracted from the recorded whole hologram, as Fig. 3 shows. The number of pixels and the pixel pitch of the piece are 512 × 512 pixels and 5.9 × 5.9 μm, respectively, and $R(x_R, 0, d)$ is the center of the piece of hologram for reconstruction. As Fig. 3 shows x_R changed as follows: 0.0 (**a**), 1.0 (**b**), 2.0 (**c**), and 3.0 mm (**d**).

We can see the reconstructed images move when the coordinates of R change along the same direction in which the reference light pulse swept, and the simulation results agree with the experimental ones from [7].

And the simulation results, as shown in Fig. 4, agree with the experimental ones from [8, 9].

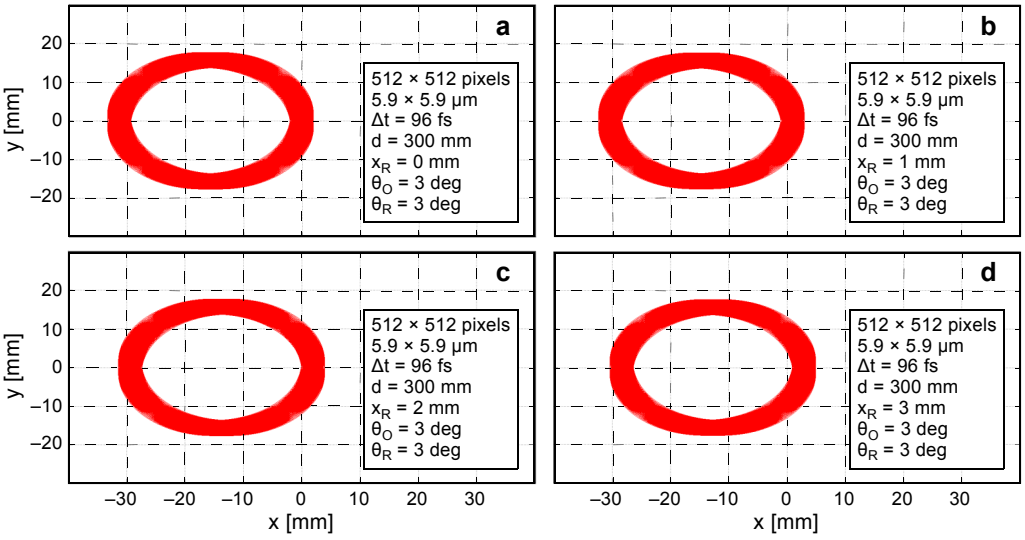

Fig. 3. Simulation results, x_R = 0.0 (**a**), x_R = 1.0 mm (**b**), x_R = 2.0 mm (**c**), and x_R = 3.0 mm (**d**).

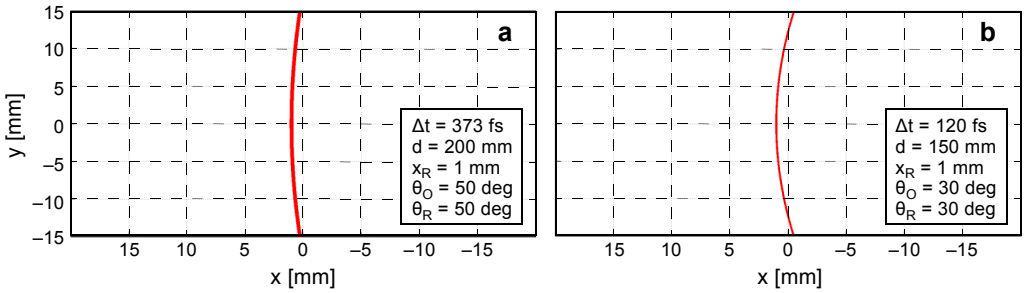

Fig. 4. Simulation results: $\Delta t = 373$ fs, $\theta_O = \theta_R = 50$ deg, $d = 200$ mm from [8] (**a**), and $\Delta t = 120$ fs, $\theta_O = \theta_R = 30$ deg, $d = 150$ mm from [10] (**b**).

In a homogeneous medium, a bright straight line is projected on the ground glass when a light pulse propagates at a moment. So the actual shape of the reconstructed images should be a bright straight line. However, when a pulse is incident to the ground glass, the transmission wavefront composes of the unaffected original wavefront and diffuse wavefront in different directions. So the aberration of the reconstructed wavefront in the transmission LIF comes from the influence of pulses scattered from different points corresponding to different time recorded simultaneously on the pulse scattered from the object plane corresponding to the accurate shape of propagating wavefront which should be a bright straight line. As shown above, the shape of the reconstructed image forms a circular or bow pattern.

According to the bending degree of arcs, as is shown in Fig. 5, we can see that with fixed θ_R the distortion of the reconstructed images decreases as θ_O increases, and with

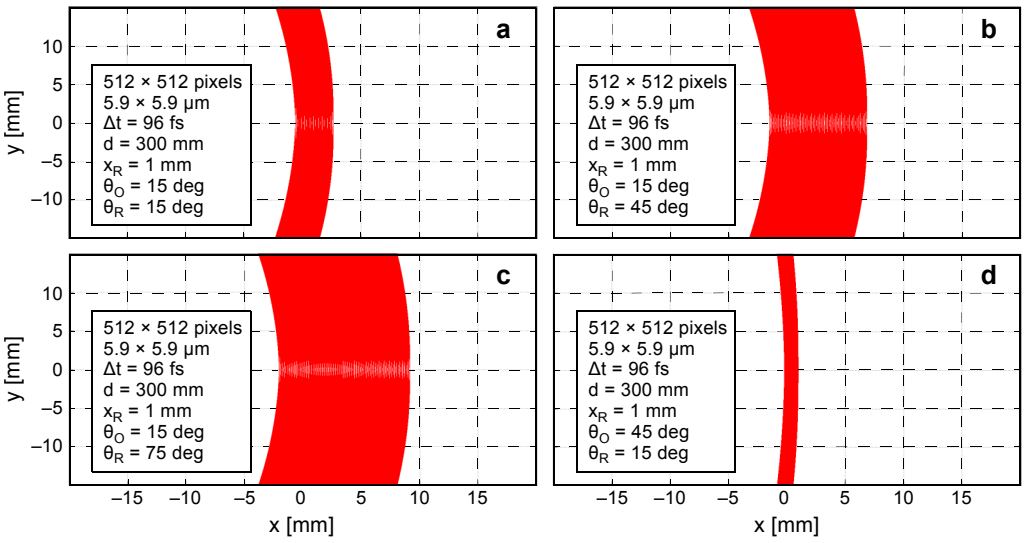

Fig. 5. Continued on the next page.

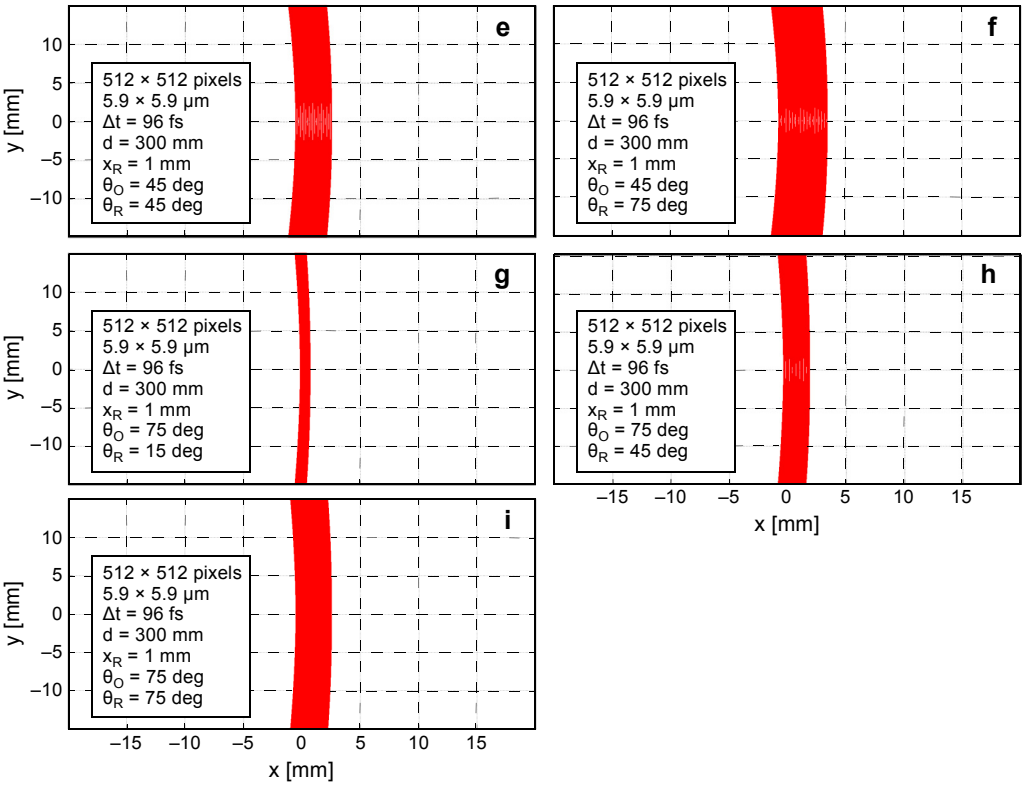

Fig. 5. Simulation results when: θ_O =15 deg, θ_R = 15 deg (**a**), θ_O =15 deg, θ_R = 45 deg (**b**), θ_O = 15 deg, θ_R =75 deg (**c**), θ_O = 45 deg, θ_R = 15 deg (**d**), θ_O = 45 deg, θ_R =45 deg (**e**), θ_O = 45 deg, θ_R =75 deg (**f**), θ_O = 75 deg, θ_R =15 deg (**g**), θ_O = 75 deg, θ_R =45 deg (**h**), and θ_O = 75 deg, θ_R =75 deg (**i**). Simulation conditions are as follows: x_R = 1 mm, Δt = 96 fs, d = 30 cm, c = 3 × 10^8 m/s, and n = 1.

fixed θ_O the change of θ_R makes no difference to the bending degree of arcs. The simulation conditions are as follows: x_R = 1 mm, Δt = 96 fs, d = 30 cm, c = 3 × 10^8 m/s, n = 1, and θ_R and θ_O changed as follows: θ_O = 15 deg, θ_R = 15 deg (**a**), θ_O = 15 deg, θ_R = 45 deg (**b**), θ_O = 15 deg, θ_R = 75 deg (**c**), θ_O = 45 deg, θ_R = 15 deg (**d**), θ_O = 45 deg, θ_R = 45 deg (**e**), θ_O = 45 deg, θ_R = 75 deg (**f**), θ_O = 75 deg, θ_R = 15 deg (**g**), θ_O = 75 deg, θ_R = 45 deg (**h**), and θ_O = 75 deg, θ_R = 75 deg (**i**). The number of pixels and the pixel pitch of the hologram piece for reconstruction are 512 × 512 pixels and 5.9 × 5.9 μm, respectively. According to the width of the reconstructed images, as shown in Fig. 5, we can see that the temporal resolution decreases as θ_R increases.

As is shown in Fig. 6, we can see the distortion of reconstructed images decreases as d increases. The simulation conditions are as follows: c = 3 × 10^8 m/s, n = 1, Δt = 96 fs, x_R = 1 mm, and θ_O = θ_R = 75 deg.

At the same time, required illuminating light intensity increases as d increases. Besides, because the illuminating light is scattered and only about 1% of the illumi-

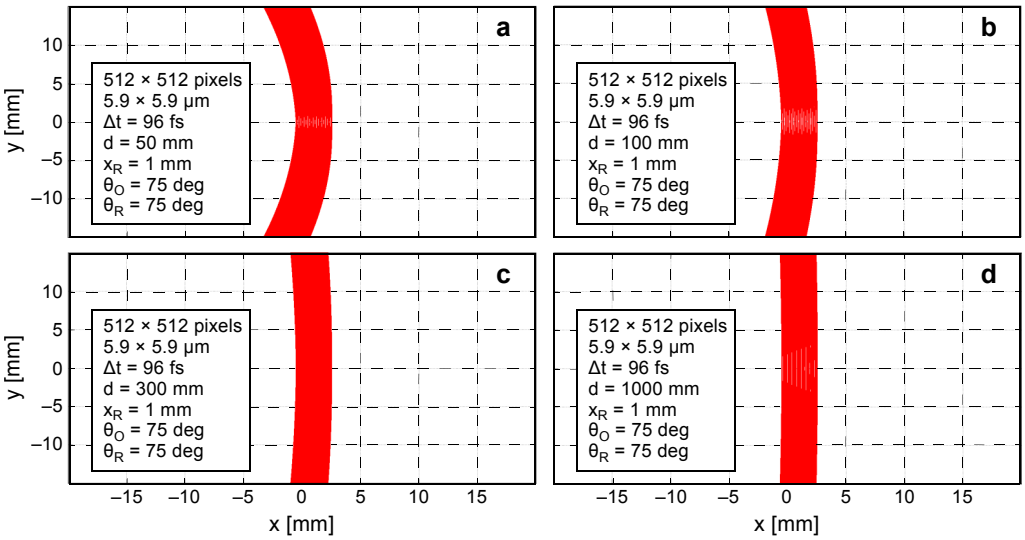

Fig. 6. Simulation results when: $d = 5$ cm (**a**), $d = 10$ cm (**b**), $d = 30$ cm (**c**), and $d = 100$ cm (**d**). Simulation conditions are as follows: $c = 3 \times 10^8$ m/s, $n = 1$, $\Delta t = 96$ fs, $x_R = 1$ mm, $\theta_O = 75$ deg, and $\theta_R = 75$ deg.

nating light intensity is recorded in transmission LIF, the ratio of the reference light intensity to the illuminating light intensity should be adjusted to the proper value.

4. The introduction of a cylindrical lens to correct the distortion partly

To obtain the actual shape of the pulse, KOMATSU *et al*. [8] proposed the following methods of image processing for the compensation of reconstructed image. 1) A coordinate transform compensating for the distortion is conducted in one reconstructed image. 2) Synthesis of the reconstructed images observed from different observation positions in the horizontal direction is conducted to compensate for the distortion. However, the phase intensity and direction of the scattered light pulse from the ground glass surface are different from each other, which makes it difficult to find an accurate image-processing algorithm for the compensation.

As discussed earlier, at a moment in a homogeneous medium, a bright straight line is projected on the ground glass when a light pulse propagates. Different dots on the straight line influence each other when recording because of the diffuse light in different directions. We defined the direction parallel to the bright straight line as the space direction, and the direction of pulse propagation along the diffuser and recording material as the time direction.

A cylindrical lens focuses the image passing through it onto a line parallel to the intersection of the surface of the lens and a plane tangent to it. As shown in Fig. 7**a**, a cylindrical lens can stretch a point of light into a line. The lens compresses the image

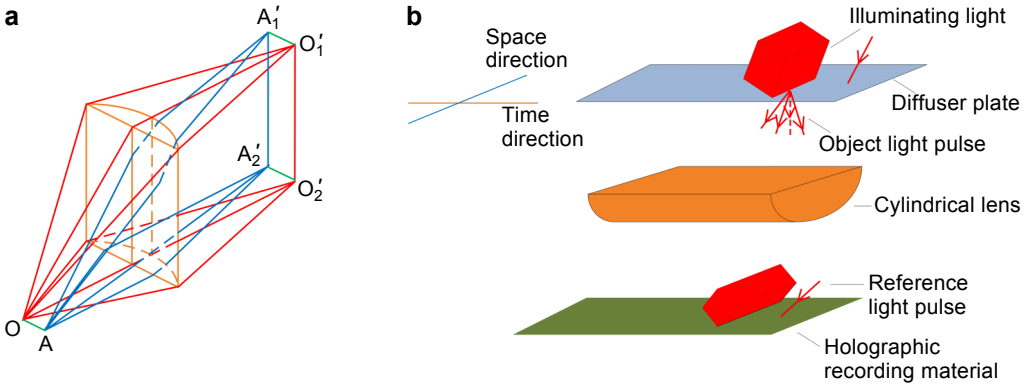

Fig. 7. Imaging optical road map of a cylindrical lens (**a**). Schematic of new arrangements (**b**).

in the direction perpendicular to this line, and leaves it unaltered in the direction parallel to it (in the tangent plane).

Theoretically, the diffuse light can be focused with large-diameter lens. Here we can place a plano-convex cylindrical lens between the diffuser plate and recording material, the flat side of the lens is parallel to the diffuser plate and recording material, and the axis of the lens was in the time direction, as shown in Fig. 7**b**. The distance between the diffuser plate and the cylindrical lens, and the cylindrical lens and the recording material is twice the focal length, respectively. Based on the Fermat principle, the diffuse light in different directions from the same point on the object plane can be refocused with lens to a point on the recording material simultaneously. So with a cylindrical lens, the influence of the scattered light in space direction can be vastly reduced, and the capability of pulse propogation recording is not influenced.

It is noteworthy that because of the imaging property of the lens, as shown in Fig. 7**b**, the reconstructed magnified image is flipped in the space direction. The height of image is related to the height and the emanative extent to the object light.

5. Simulation of changing wavefront recording

Assume that the pulse propagates in a medium with the refractive index distribution $n_y = n_0 - ay^2$, so the cross-section of the object light pulse wavefront on the object plane changes during propagation. Assume the cross-section at position 0 is a straight line, as shown in Fig. 8, and the illuminating pulse and reference pulse propagates along the x-axis. The coordinates of A should satisfy the equation as follows:

$$x = \frac{tc}{n}\sin(\theta_O) \tag{3}$$

All the symbols defined are the same as in Fig. 2.

Assume that the object light pulse scattered at 0 propagates in the z-direction and the reference light pulse arrived at R_0 simultaneously. And the object light pulse scat-

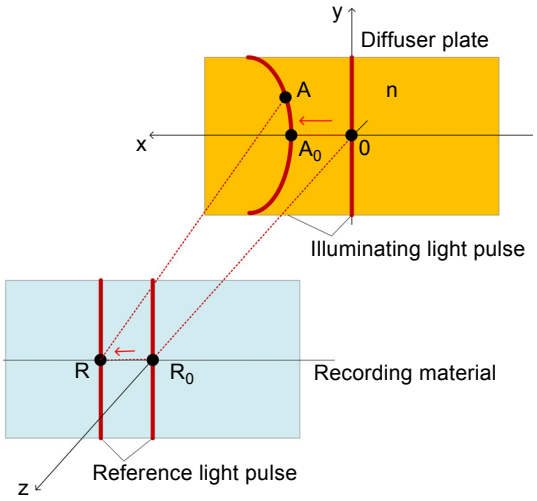

Fig. 8. Simulation model.

tered at A and the reference light pulse simultaneously arrive at R. According to the principle that the optical path length of the object light pulse and the reference light pulse is equal, we can obtain that

$$d + L_{R_0-R}\sin(\theta_R) = nL_{0-A}\sin(\theta_O) + L_{A-R} \tag{4}$$

Assume the simulation conditions are as follows: d = 30 cm, $\theta_O = \theta_R$ = 75 deg, $c = 3 \times 10^8$ m/s, n_0 = 1.5, a = 2000, y_R = 0. As Figure 9**a** shows, from left to right, x_R changed from 1.5104 to 22.656 mm. We can see the reconstructed wavefront move when x_R changes along the same direction in which the reference light pulse swept, and the reconstructed images agree with the simulation ones, as shown in Fig. 9**b**, from left to right (t changed from 0 to 70 ps).

As shown in Fig. 10, we can see that the difference between the images reconstructed from recording dots $R(x_R, y_R, d)$ with same x_R and different y_R decreases as θ_O and

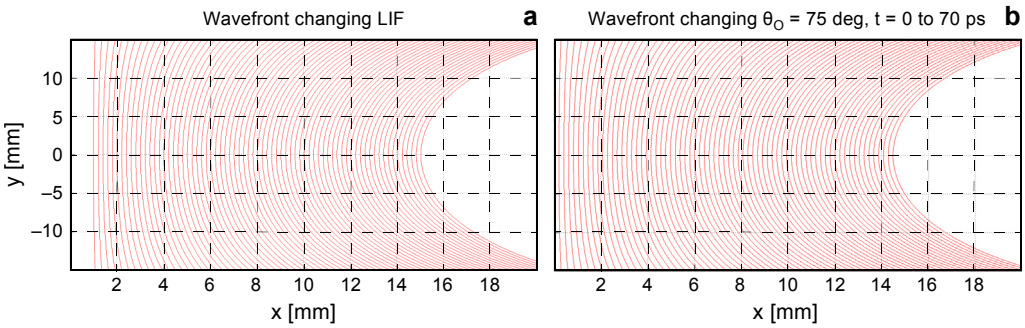

Fig. 9. Wavefront changes during propagation. LIF reconstruction (**a**), and simulation of propagating wavefront (**b**).

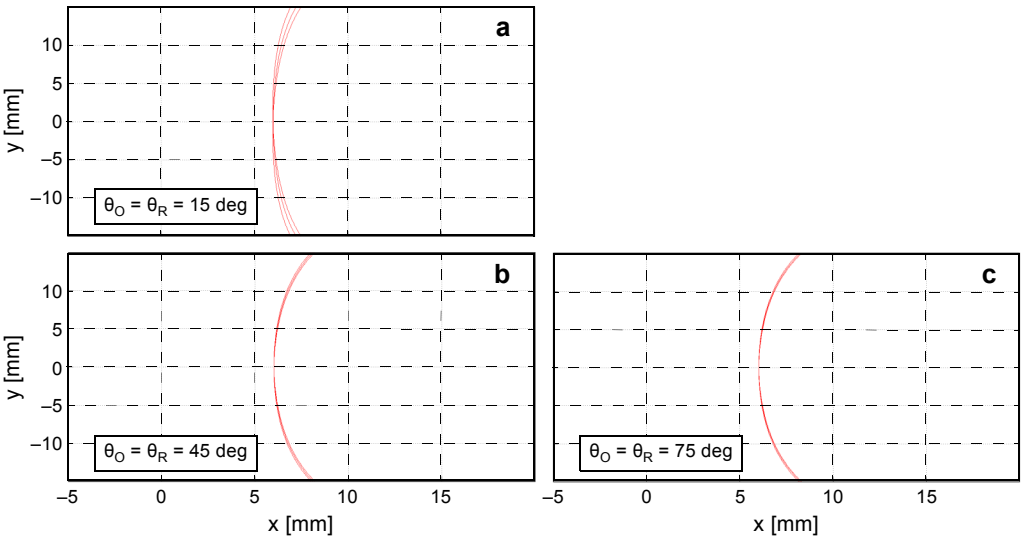

Fig. 10. Wavefront reconstructed from recording dots $R(x_R, y_R, d)$ with fixed x_R and different y_R; $\theta_O = \theta_R = 15$ deg (**a**), $\theta_O = \theta_R = 45$ deg (**b**), and $\theta_O = \theta_R = 75$ deg (**c**).

θ_R increases. The simulation conditions are: d = 30 cm, $c = 3 \times 10^8$ m/s, n_0 = 1.5, a = 2000, x_R = 9.0624 mm, and from left to right, y_R changed as follows: –1.5104, 0, and 1.5104 mm; θ_O and θ_R changed as follows: $\theta_O = \theta_R$ = 15 deg, $\theta_O = \theta_R$ = 45 deg and $\theta_O = \theta_R$ = 75 deg.

Then we obtained the reconstructed images of femtosecond light pulse propagation from pieces extracted from recorded hologram, as shown in Fig. 11. The number of pixels and the pixel pitch of the hologram piece are 512 × 512 pixels and 5.9 × 5.9 μm, respectively, and $R(x_R, y_R, d)$ is the center of the piece of the hologram for reconstruction. Figures 11**a**–11**c** show the wavefront reconstructed in LIF; x_R changed as follows: 3.0208 (**a**), 6.0416 (**b**), and 9.0624 mm (**c**). Figures 11**d**–11**f** show the wavefront of different time slice of pulse propagation; t changed as follows: from 0 to 10 ps (**d**), from 10 to 20 ps (**e**), and from 20 to 30 ps (**f**). And we can see that the wavefront reconstructed in LIF coincides with that of the ultrashort pulse propagation.

6. Summary

In summary, the distortion of reconstructed wavefront in LIF holography arises from the pulses scattered from each point composing the reconstructed image do not perfectly correspond to the pulse scattered on the object plane at the same time in the recording. Based upon the simulation and comparison, as to the wavefront invariable during the propagation, we can reach the conclusion that the distortion of reconstructed images decreases as θ_O and d increase, so we should set the value of θ_O and d as large as possible to record more accurately. Meanwhile, the required illuminating light intensity and the ratio of the illuminating light intensity to the reference light intensity

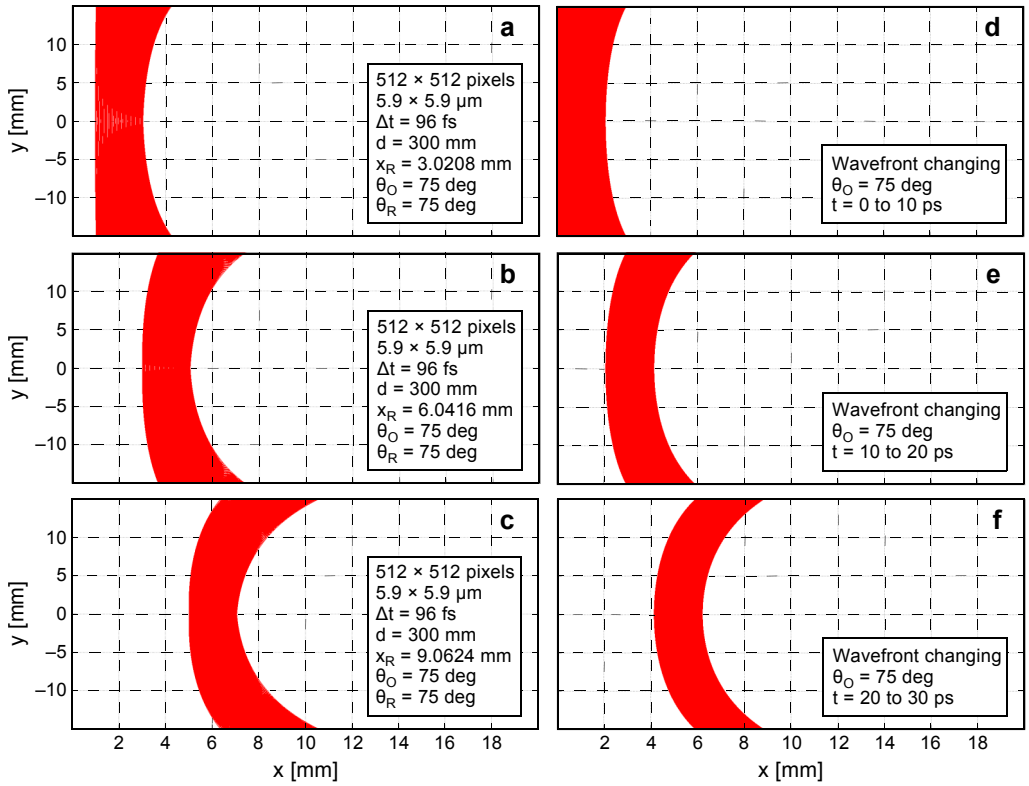

Fig. 11. Wavefront changes during propagation. Wavefront reconstructed in LIF: x_R = 3.0208 mm (**a**), x_R = 6.0416 mm (**b**), and x_R = 9.0624 mm (**c**). Wavefront of different time slice of pulse propagation t: from 0 to 10 ps (**d**), from 10 to 20 ps (**e**), and from 20 to 30 ps (**f**).

should be adjusted properly. And as θ_R increases, the distortion remains fixed and the temporal resolution decreases.

In addition to the selection of relevant parameters, a cylindrical lens scheme was proposed to rectify the distortion partly in space direction. Furthermore, the simulation of wavefront changing during propagation recording was made. However, to confirm the results of the model and scheme, a more complete analysis and additional experimental investigations are suggested for further studies.

Acknowledgements – This research was supported by the National Natural Science Foundation of China under Grant No. 61027014 and the Project of Science and Technology Research Fund of Shenzhen Municipality (JCYJ20130329140654277).

References

[1] Abramson N., *Light-in-flight recording by holography*, Optics Letters **3**(4), 1978, pp. 121–123.

[2] Abramson N., *Optical fiber tested using light-in-flight recording by holography*, Applied Optics **26**(21), 1987, pp. 4657–4659.

[3] CARLSSON T.E., NILSSON B., GUSTAFSSON J., *System for acquisition of three-dimensional shape and movement using digital light-in-flight holography*, Optical Engineering **40**(1), 2001, pp. 67–75.
[4] HERRMANN S.F., HINSCH K.D., *Light-in-flight holographic particle image velocimetry for wind-tunnel applications*, Measurement Science and Technology **15**(4), 2004, pp. 613–621.
[5] SPEARS K.G., SERAFIN J., ABRAMSON N.H., ZHU X., BJELKHAGEN H., *Chrono-coherent imaging for medicine*, IEEE Transactions on Biomedical Engineering **36**(12), 1989, pp. 1210–1221.
[6] KUBOTA T., KOMAI K., YAMAGIWA M., AWATSUJI Y., *Moving picture recording and observation of three-dimensional image of femtosecond light pulse propagation*, Optics Express **15**(22), 2007, pp. 14348–14354.
[7] KAKUE T., TOSA K., YUASA J., TAHARA T., AWATSUJI Y., NISHIO K., URA S., KUBOTA T., *Digital light -in-flight recording by holography by use of a femtosecond pulsed laser*, IEEE Journal of Selected Topics in Quantum Electronics **18**(1), 2012, pp. 479–485.
[8] KOMATSU A., AWATSUJI Y., KUBOTA T., *Dependence of reconstructed image characteristics on the observation condition in light-in-flight recording by holography*, Journal of the Optical Society of America A **22**(8), 2005, pp. 1678–1682.
[9] YAMAMOTO S., TAKIMOTO T., TOSA K., KAKUE T., AWATSUJI Y., NISHIO K., URA S., KUBOTA T., *Moving picture recording and observation of femtosecond light pulse propagation using a rewritable holographic material*, Nuclear Instruments and Methods in Physics Research Section A **646**(1), 2011, pp. 200–203.

Received August 5, 2016
in revised form September 18, 2016